

## Article

# Power Control Strategy for a Ferry's DC Power System Using Supercapacitors

Qinsheng Yun <sup>1,2</sup>, Lijun Fu <sup>3</sup>, Li Cheng <sup>4</sup>  and Xiangjun Wang <sup>1,\*</sup>

<sup>1</sup> School of Electrical Engineering, Naval University of Engineering, Wuhan 430033, China; yunqinsheng@126.com

<sup>2</sup> Shanghai Marine Diesel Engine Research Institute, Shanghai 201111, China

<sup>3</sup> State Key Laboratory of Electromagnetic Energy, Naval University of Engineering, Wuhan 430033, China; lijunfu2006@sina.cn

<sup>4</sup> School of Naval Architecture, Ocean and Energy Power Engineering, Wuhan University of Technology, Wuhan 430063, China; chengli@whut.edu.cn

\* Correspondence: wxjnue@163.com

**Abstract:** Integrated power systems are gaining popularity in the field of power systems and DC integrated power systems are considered promising for electric propulsion ships due to their simple grid topology, low fuel consumption, and easy access to new energy sources. However, the dynamic response characteristics of the power plant can be compromised when a variable speed generator is used in a DC power system, despite achieving energy savings. In this research, we investigate the power control strategy of a specific type of a ferry's DC power plant. We establish a mathematical model and a Matlab/Simulink-based simulation model to analyze the performance of the proposed strategy. The research utilizes the fast charging and discharging advantages of supercapacitor storage devices to compensate for the dynamic impact delay of the power output when using the variable speed generator set. Additionally, an improved DC bus voltage droop control method that incorporates voltage compensation is proposed to mitigate problems related to large bus voltage fluctuations under sudden load change conditions, enabling better load distribution between different power sources. The simulation results confirm the effectiveness of the proposed strategy in optimizing the speed-seeking method of the variable speed diesel engine sets matching with the supercapacitor, and its positive impact on the dynamic performance of the propulsion system is demonstrated under variable load conditions resulting from ferry operations.

**Keywords:** electric propulsion; DC network; variable speed generation; supercapacitor; droop control



**Citation:** Yun, Q.; Fu, L.; Cheng, L.; Wang, X. Power Control Strategy for a Ferry's DC Power System Using Supercapacitors. *Electronics* **2023**, *12*, 2878. <https://doi.org/10.3390/electronics12132878>

Academic Editor: Fabio Corti

Received: 8 May 2023

Revised: 6 June 2023

Accepted: 20 June 2023

Published: 29 June 2023



**Copyright:** © 2023 by the authors. Licensee MDPI, Basel, Switzerland. This article is an open access article distributed under the terms and conditions of the Creative Commons Attribution (CC BY) license (<https://creativecommons.org/licenses/by/4.0/>).

## 1. Introduction

In recent years, technological advancements in power electronics technology, new energy systems, and control theory have significantly facilitated the development of marine electric propulsion systems. As a result, the “Integrated Power System” (IPS) [1] has been further developed. Deploying an IPS strategy merges the propulsion and power systems of a vessel and enables efficient control of the entire vessel's energy, as well as facilitating flexible access to various renewable energy sources.

The primary types of integrated power systems present in ships are AC power systems and DC power systems [2]. Currently, the dominant type is the AC power system, which benefits from mature technology and high reliability. Nevertheless, the traditional AC generator necessitates complex control and imposes additional constraints for grid connection. On the other hand, the DC power system provides lower cost and higher reliability, accomplished through reduced emissions, lower noise, and lower wear while permitting diesel or gas turbine generators of different capacities and speeds to run in parallel to the DC bus [3]. Furthermore, DC network technology makes it convenient to connect energy storage devices such as supercapacitors, lithium batteries, and alternate forms of energy like

fuel cells. Consequently, DC networks are rapidly becoming a research hotspot. As opposed to AC networks, DC networks encounter no issues with reactive power, AC/DC conversion losses, frequency, and voltage phasing, which ultimately provide greater security and reliability of power supply [4].

In circumstances of sudden loading and unloading, diesel generators tend to have slow and inadequate dynamic responses, rendering them ineffective in coping with impulsive load changes. Supercapacitors, when employed, can facilitate power balancing between the generating unit and the load, enhance system inertia, stabilize system operations, and efficiently adjust diesel workloads within high-efficiency ranges. Consequently, the energy efficiency of the system improves and the service life of the diesel generator extends. In the civil sector, a DC electric propulsion system, including a variable speed generator set equipped with supercapacitors, proves suitable for variable load conditions such as ferries, tugs, and engineering vessels.

Direct current networks are a feasible solution for ships powered by multiple sources of energy; however, matching the power output between these sources is vital as it affects the overall performance of the ship. The study of energy management strategies is, therefore, imperative for the integration of power systems. The power control strategy for integrated power systems is informed by the intricate and ever-changing working conditions of ships, considering the distinct characteristics of various energy sources to achieve smart distribution, generation, and consumption of ship power [5,6]. The goal is to improve energy efficiency and system stability. Efficient power management of a hybrid ship powered by multiple energy sources requires the optimization of several factors such as the diesel generator's optimal performance point, state of charge of the energy storage device, and other considerations to solve the problems associated with non-linearity and constraint optimization to achieve the optimal energy allocation. The effectiveness of power management strategies is directly proportional to considerations such as energy efficiency, fuel economy, emissions, power dynamics, and service life [7].

Currently, two primary challenges affect DC power systems matched with supercapacitors. Firstly, optimizing the speed of the power-generating diesel engine according to load variations to improve ship energy efficiency while preserving equipment lifespan. Secondly, constructing a dynamic energy management strategy for the multi-source heterogeneous energy coupled system and devising a control strategy keeping in mind the importance of maintaining grid voltage stability and precise control over the output power of individual energy sources.

A literature review was conducted to comprehensively analyze the effects of supercapacitor banks as energy storage systems in renewable energy grids with high-voltage DC buses [8]. The results demonstrated that supercapacitor banks have a smoother dynamic response, more efficient and flexible power management, higher voltage stability, longer battery bank life, and operational protection of equipment affected by current peaks. The literature [9] corrected the theoretical minimum fuel consumption speed in the universal characteristic curve by incorporating actual parameters such as the temperature of the diesel engine. DC microgrid stability was addressed in [10] by establishing a hybrid potential function theory-based criterion that considers battery state charge state and quantitatively analyzing the power boundary of system operation. Furthermore, [11] introduced a method for deriving stability criteria for DC microgrid systems with improved droop control, while also addressing the load's large disturbance stability problems. Additionally, [12] reduced the deviation of the actual output power of the distributed power supply from the desired output power by introducing a sample keeper in the droop control of the distributed power supply and effectively improving the bus voltage quality. Though the aforementioned studies have successfully addressed bus voltage instability, there is insufficient research on control strategies to overcome the significant bus fluctuations associated with marine DC networks that employ a variable-speed diesel generator.

This paper investigates and proposes a power control strategy for marine DC networks with multiple power sources. The case study is conducted on an electric power configura-

tion of a ferry for ZhenYang Ferry Company, which often operates on varying load profiles. In the proposed solution, the hybrid DC power system cored by using supercapacitor to assist the variable speed diesel generators is proposed. A bidirectional DC/DC converter is introduced between the supercapacitor and the DC bus, reducing the voltage level requirement of the supercapacitor and facilitating the charging and discharging control of the supercapacitor. An improved droop method is introduced to achieve the optimal power balance between the multiple the power sources while improving the quality of power supply for this hybrid system.

## 2. Modelling of a Ship's DC Grid Power System

The performance of a ship's DC grid power system is heavily influenced by its topology, equipment parameters, and energy management strategy. This section introduces the vessel and the configuration of its DC grid power system, followed by an analysis of the mathematical model of each device. Based on this analysis, a system simulation model is created to test the control strategy presented in Section 4 via simulation experiments.

### 2.1. Target Vessel

Figure 1 shows the topology of the DC network of the target ship. The system includes two 380 kW variable speed diesel generator sets, a DC switchboard, a 9.5 kWh supercapacitor, two 350 kW propulsion motors, and a power management system. The DC switchboard comprises a DC busbar, a rectifier unit, an inverter unit, a bi-directional DC/DC converter, and a protection device among others. After power generation, the variable-speed diesel generator sets are connected to the DC busbar via the rectifier unit. The supercapacitor uses a bi-directional DC/DC converter to link to the DC busbar while the thrust motor and other equipment are powered by the DC busbar through the inverter unit. The busbar's voltage rating is 750 V. The specific parameters of the system are listed in Table 1.

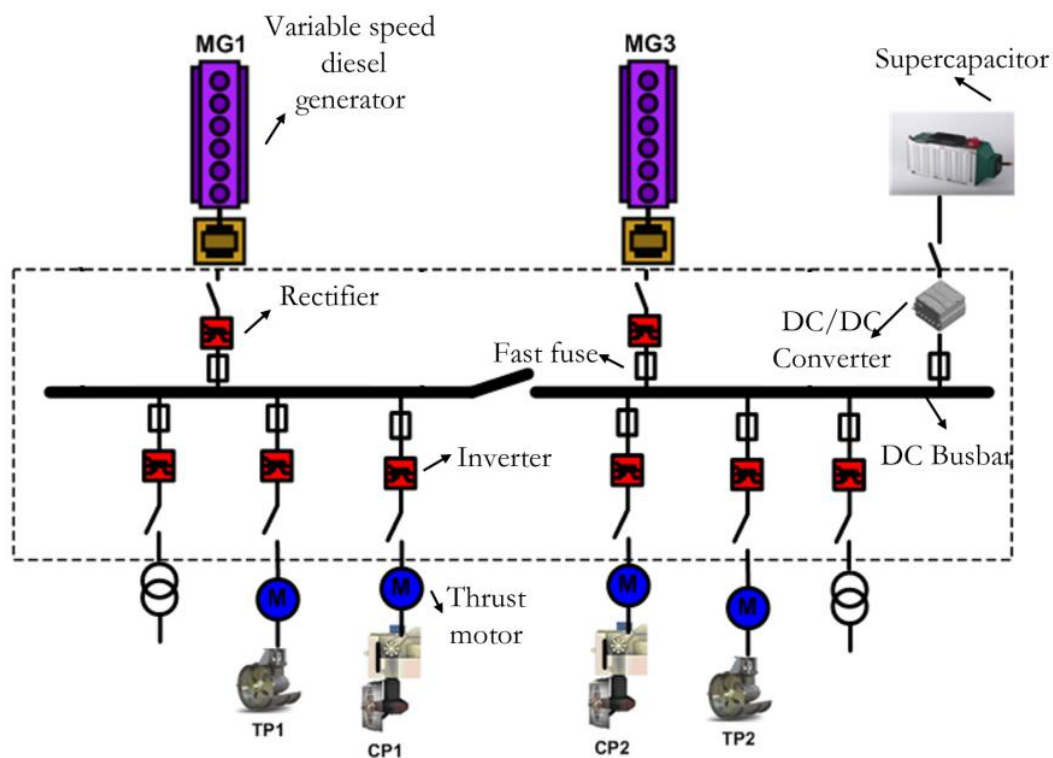


Figure 1. Configuration of DC network.

**Table 1.** Target vessel parameters.

Parameter	Value	Parameter	Value
Total length	69.51 m	Ship length	57.60 m
Full waterline length	59.82 m	Ship width	15.40 m
Maximum ship width	15.70 m	Depth	3.50 m
Maximum ship height	21.55 m	Construction type	Transversely system of framing
No-load draught	1.79 m	No-load displacement	745.90 t
Full draught	2.35 m	Full-load Displacement	1213.65 t
Diesel engine	412 kW/1800 r/min	Asynchronous generators	380 kW/440 V
Supercapacitor capacity	9.5 kWh	Propulsion motors	350 kW/400 V

## 2.2. Diesel Engine Model

The diesel engine serves as the prime mover, powering the asynchronous generator to produce electricity. Both the torque and speed characteristics of the diesel engine have been analyzed and a dynamic model is built. The mechanical torque dynamic equation is represented as Equation (1):

$$T_d = T_g + T_f + J \frac{d\omega}{dt}, \quad (1)$$

where  $T_d$  and  $T_f$  are the mechanical torque and friction torque of the diesel engine, respectively;  $T_g$  is generator electromagnetic torque;  $J$  is the rotational inertia;  $\omega$  is the crankshaft's angular velocity.

During operation, the mechanical torque of the diesel engine,  $T_d$ , is primarily a function of the engine's speed,  $n$ , and the output shaft's offset of electronic governor,  $L$ . As such, it can be represented as a mathematical function,  $T_d = f_1(n, L)$ . On the other hand, the load torque of the generator,  $T_g$ , is mainly affected by the diesel engine speed,  $n$ , and the load power,  $P_L$ . It is represented as a function,  $T_g = f_2(n, P_L)$ .

The speed characteristics of diesel engines are nonlinear, hence, to enable accurate analysis, they can be approximated as a series of linear segments. The mathematical model of the diesel engine, developed in this research, caters to both turbocharged and naturally aspirated diesel engines. The expression of  $T_d$ , obtained by combining the speed characteristics and regulation characteristics of the diesel engine, is shown as:

$$T_d = k_i n + b_i - L \frac{M_1^e}{L_e}, \quad (2)$$

where  $i = 1, 2, \dots, x$ , for each speed segment, the coefficients  $k_i, b_i$  assume different values;  $M_1^e$  is the maximum torque of diesel engine;  $L_e$  is the maximum travel of the electronic governor's output shaft.

When load changes, the original dynamic balance of torque is broken and the speed changes. The discrete equation of the above equation is as follows:

$$J \frac{d(\omega + \Delta\omega)}{d(t + \Delta t)} = (T_d + \Delta T_d) - (T_g + \Delta T_g) - (T_f + \Delta T_f), \quad (3)$$

where  $\Delta$  represents the amount of variation of each parameter.

## 2.3. PID Speed Controller for Diesel Engines

Figure 2 depicts the schematic diagram of the diesel engine's speed control system. It involves closed-loop speed control through a speed feedback unit and sends the speed signal to the comparator to determine the variance with the reference speed. The speed regulation unit is responsible for producing an output signal, which is fed to the actuator control by the PID controller to adjust the diesel engine's fuel injection to change the output torque for achieving speed control.

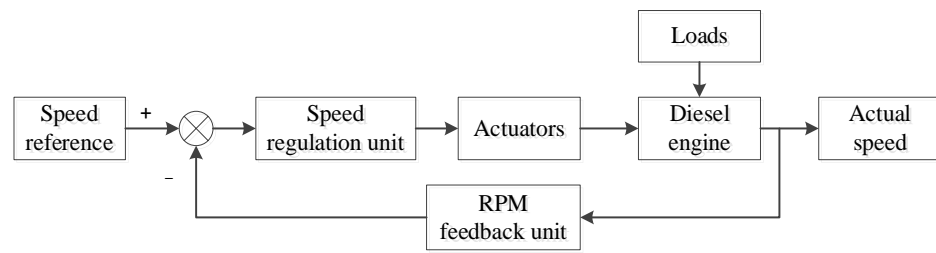


Figure 2. Diagram of speed regulation system for diesel engine.

The mathematical model of the PID controller in the speed regulation unit is as follows:

$$u(t) = K_P \left[ e(t) + \frac{1}{T_I} \int_0^t e(\tau) d\tau + T_D \frac{de(t)}{dt} \right], \tag{4}$$

where  $u(t)$  is the control signal of injection;  $e(t)$  is the speed deviation;  $K_P$ ,  $T_I$ , and  $T_D$  are the PID control parameters.

The actuator can be simplified to a first-order inertial element and a proportional element, whose mathematical model can be shown as

$$W(s) = \frac{F(s)}{u(s)} = \frac{K}{1 + T(s)}, \tag{5}$$

where  $F(s)$  is the fuel rack position;  $K$  is the proportionality coefficient;  $T(s)$  is the time constant of actuator inertia.

#### 2.4. Asynchronous Generator Model

To facilitate the analysis, the mathematical model of the three-phase asynchronous generator is represented by the  $dq$  rotating coordinate system and the mathematical equations of voltage and torque are expressed.

In a three-phase asynchronous generator, the flux chain in the  $dq$  coordinate system can be expressed as follows:

$$\begin{bmatrix} \psi_{sd} \\ \psi_{sq} \\ \psi_{rd} \\ \psi_{rq} \end{bmatrix} = \begin{bmatrix} L_s & 0 & L_m & 0 \\ 0 & L_s & 0 & L_m \\ L_m & 0 & L_r & 0 \\ 0 & L_m & 0 & L_r \end{bmatrix} \begin{bmatrix} i_{sd} \\ i_{sq} \\ i_{rd} \\ i_{rq} \end{bmatrix}, \tag{6}$$

where  $\psi_{sd}$ ,  $\psi_{sq}$  are, respectively the stator flux's  $dq$  components;  $\psi_{rd}$  and  $\psi_{rq}$  are the rotor flux's  $dq$  components, respectively;  $L_s$  is the stator self-inductance;  $L_r$  is the rotor self-inductance;  $L_m$  is the stator-rotor mutual inductance;  $i_{sd}$  and  $i_{sq}$  are the stator current's  $dq$  components, respectively;  $i_{rd}$  and  $i_{rq}$  are the rotor current's  $dq$  components, respectively.

The stator voltage equation can be expressed as follows:

$$U_s = R_s i_s + L_s \frac{di_s}{dt} + \frac{dL_s}{d\theta} \omega_r i_s. \tag{7}$$

The rotor voltage equation can be expressed as follows:

$$U_r = R_r i_r + L_r \frac{di_r}{dt} + \frac{dL_r}{d\theta} \omega_r i_r, \tag{8}$$

where  $U_s$  and  $U_r$  are the instantaneous phase voltage of the stator and rotor;  $R_s$  and  $R_r$  are the resistance of the stator and rotor;  $\omega_r$  is the rotor angular velocity;  $\theta$  is the angle between stator and rotor.

The voltage equations of asynchronous generator in  $dq$  coordinate system as below:

$$\begin{bmatrix} u_{sd} \\ u_{sq} \\ u_{rd} \\ u_{rq} \end{bmatrix} = \begin{bmatrix} R_s + L_s p & -\omega_1 L_s & L_m p & -\omega_1 L_m \\ \omega_1 L_s & R_s + L_s p & \omega_1 L_s & L_m p \\ L_m p & -\omega_s L_m & R_r + L_r p & -\omega_s L_r \\ \omega_s L_m & L_m p & \omega_s L_r & R_r + L_r p \end{bmatrix} \begin{bmatrix} i_{sd} \\ i_{sq} \\ i_{rd} \\ i_{rq} \end{bmatrix}, \tag{9}$$

where,  $\omega_1$  is the synchronous angular velocity of stator frequency;  $\omega_s = \omega_1 - \omega_r'$ ,  $\omega_s$  is the slip of the asynchronous motor.  $\omega_z$  is the stator's angular speed;  $p$  is the coefficient of differentiation.

The electromagnetic torque equation and the equation of motion are indispensable equations in the analysis of the dynamic response and system stability of asynchronous motors.

The equation for the electromagnetic torque of an asynchronous motor is shown as

$$T_g = \frac{3}{2} P_g \frac{L_m}{L_r} \psi_{rd} i_{sq}, \tag{10}$$

where  $P_g$  refers to the polar pairs.

The motion equation of the asynchronous motor is shown as

$$\left( \frac{1}{P_g} \right) J' \frac{d\omega_r}{dt} = T_g - T_L, \tag{11}$$

where  $T_L$  is the load torque.  $J'$  is the generator's rotational inertia.

The dynamic equations of the asynchronous generator are constructed according to the vector transformation rule, with the voltage vector  $u = [u_d, u_q]^T \in R^2$  as the input quantity.  $u_d$  and  $u_q$  are the stator voltage  $dq$  components, respectively,  $\omega_e$  is the electric angular velocity. The dynamic equations of the asynchronous generator in the  $dq$  coordinate system are shown as

$$\begin{cases} \frac{di_{sd}}{dt} = -\left( \frac{R_s}{\sigma L_s} + \frac{L_m^2 R_r}{\sigma L_s L_r^2} \right) i_{sd} + \omega_r i_{sq} + \frac{L_m R_r}{\sigma L_s L_r} \psi_{rd} + \frac{L_m}{\sigma L_s L_r} \omega_e \psi_{rq} + \frac{1}{\sigma L_s} u_d \\ \frac{di_{sq}}{dt} = -\omega_r i_{sd} - \left( \frac{R_s}{\sigma L_s} + \frac{L_m^2 R_r}{\sigma L_s L_r^2} \right) i_{sq} - \frac{L_m}{\sigma L_s L_r} \omega_e \psi_{rd} + \frac{L_m R_r}{\sigma L_s L_r} \psi_{rq} + \frac{1}{\sigma L_s} u_q \\ \frac{d\psi_{rd}}{dt} = \frac{L_m R_r}{L_r} i_{sd} - \frac{R_r}{L_r} \psi_{rd} + (\omega_r - \omega_e) \psi_{rq} \\ \frac{d\psi_{rq}}{dt} = \frac{L_m R_r}{L_r} i_{sq} - (\omega_r - \omega_e) \psi_{rq} - \frac{R_r}{L_r} \psi_{rd} \\ \frac{d\omega_e}{dt} = \frac{P_g}{J'} (T_d - T_g - T_f) = \frac{P_g}{J'} \left( T_d - \frac{3P_g L_m}{2L_r} (\psi_{rd} i_{sq} - \psi_{rq} i_{sd}) - T_f \right) \end{cases}, \tag{12}$$

where,  $R_s$  and  $R_r$  are the stator and rotor resistance, respectively,  $L_s$ ,  $L_r$ , and  $L_m$  are the self-inductance and mutual inductance of the stator and rotor, respectively;  $J'$  is the generator's rotational inertia and  $\omega_r$  is the rotor angular velocity.  $\sigma = 1 - L_m^2 / (L_s L_r)$  is the leakage coefficient;  $T_g$  is the electromagnetic torque;  $T_d$  is the mechanical torque. Given the rotor flux chain is oriented on the d-axis of the reference coordinate system, the rotor flux chain has only the d-axis component, and no q axis component, which is  $\psi_{rq} = 0$ . Substituting  $\psi_{rq} = 0$  into the fourth equation in Equation (12) results in

$$\omega_r = \omega_e + \frac{L_m R_r}{L_r} \frac{i_{sq}}{\psi_{rd}}. \tag{13}$$

Substituting Equation (13) into Equation (12), we can get Equation (14):

$$\begin{cases} \frac{di_{sd}}{dt} = -\left( \frac{R_s}{\sigma L_s} + \frac{L_m^2 R_r}{\sigma L_s L_r^2} \right) i_{sd} + \omega_e i_{sq} + \frac{L_m R_r i_{sq}^2}{L_r \psi_{rd}^2} + \frac{L_m R_r}{\sigma L_s L_r} \psi_{rd} + \frac{1}{\sigma L_s} u_d \\ \frac{di_{sq}}{dt} = -\left( \frac{R_s}{\sigma L_s} + \frac{L_m^2 R_r}{\sigma L_s L_r^2} \right) i_{sq} - \left( \omega_e + \frac{L_m R_r i_{sq}}{L_r \psi_{rd}} \right) i_{sd} - \frac{L_m}{\sigma L_s L_r} \omega_e \psi_{rd} + \frac{1}{\sigma L_s} u_q \\ \frac{d\psi_{rd}}{dt} = -\frac{R_r}{L_r} \psi_{rd} + \frac{L_m R_r}{L_r} i_{sd} \\ \frac{d\omega_e}{dt} = \frac{P_g}{J'} (T_d - T_g - T_f) = \frac{P_g}{J'} \left( T_d - \frac{3P_g L_m}{2L_r} \psi_{rd} i_{sd} - T_f \right) \end{cases} \tag{14}$$

Rotor field orientation simplified the speed and flux equations. The flux chain amplitude of the motor is the d-axis flux, which is solely determined by the d-axis current. When the flux remains constant, the q-axis current determines the electromagnetic torque, thereby achieving a steady-state decoupling between the axes. Consequently, control of the motor can be achieved using only current.

### 2.5. Supercapacitor Model

This paper uses the supercapacitor equivalent model from Matlab/Simulink. The terminal voltage of the supercapacitor bank is  $U_c$ . The expression of its stored energy  $E_{sc}$  function is shown as

$$E_{sc} = \frac{1}{2} C_{sc} U_c^2, \quad (15)$$

where  $C_{sc}$  is the capacitance capacity of the supercapacitor.

In the practice application, the supercapacitor charging cut-off voltage is  $U_{scmax}$  and discharging cut-off voltage is  $U_{scmin}$ , and its total available energy  $E_{sc}'$  function expression is as follows:

$$E_{sc}' = \frac{1}{2} C_{sc} (U_{scmax}^2 - U_{scmin}^2). \quad (16)$$

Incorporating supercapacitors into a DC power system can enhance power quality and mitigate bus voltage fluctuations by storing and discharging energy through the supercapacitor in response to frequent load variations during maneuvering operations. For the target vessel, the Aowei S545V19-K8-A system was selected, consisting of 24 standard modules of model MUCK24V2870 in series, each containing 18 high-energy supercapacitors arranged in three parallel and six series. The operating voltage range of each group of standard modules is 410~547 V.

### 2.6. Rectifier Model

Rectifiers are fundamental to electrical systems; Pulse-width modulated (PWM) rectifiers, in particular, offer high voltage utilization rate and low current harmonic distortion rate [13], thus making them well-suited for DC ship power systems.

Define the three-phase rectifier bridge switching functions  $S_a$ ,  $S_b$ , and  $S_c$  which can only take 1 or 0. The switching function of the three-phase rectifier bridge can either be 1 or 0. If it is 1, the upper bridge arm of the corresponding phase is set to the "on" state, and the lower bridge arm is set to the "off" state. If it is 0, the upper bridge arm of the target phase is switched off while the lower bridge arm is switched on. By analyzing the input and output sides of the grid using Kirchhoff's law, a mathematical model for the PWM rectifier in the ABC coordinate system can be derived; the mathematical model for the PWM rectifier in the coordinate system can be obtained as follows:

$$\begin{cases} L' \frac{di_a}{dt} = u_a - Zi_a - u_{DC} (S_a - \frac{1}{3} \sum_{i=a,b,c} S_i) \\ L' \frac{di_b}{dt} = u_b - Zi_b - u_{DC} (S_b - \frac{1}{3} \sum_{i=a,b,c} S_i) \\ L' \frac{di_c}{dt} = u_c - Zi_c - u_{DC} (S_c - \frac{1}{3} \sum_{i=a,b,c} S_i) \\ C \frac{du_{DC}}{dt} = i_{DC} = S_a i_a + S_b i_b + S_c i_c - \frac{u_{DC}}{R_L} \end{cases} \quad (17)$$

where  $u_a$ ,  $u_b$ , and  $u_c$  are the electromotance of the three-phase AC grid on the AC side;  $L'$  is the AC input inductance;  $Z$  is the AC line impedance;  $i_a$ ,  $i_b$ , and  $i_c$  are the AC load current;  $i_{DC}$  and  $u_{DC}$  are the current and voltage of the DC bus on the DC side, respectively.

### 2.7. Bidirectional DC/DC Model

Bidirectional DC/DC converters enable a bidirectional flow of energy by controlling electronic power switches. DC/DC voltage converters can be divided into two categories depending on whether they are electrically isolated or not. In isolated converters, the voltage side is galvanically isolated, that is, isolated by a transformer, while non-isolated converters do not have a transformer. Isolated DC/DCs are mainly used for high-power

applications, in this paper, a new isolated three-phase bridge DC/DC converter is modeled. The bidirectional DC/DC converter is created by combining a boost converter with a buck converter in cascade, allowing it to function as a step-up or step-down converter that can either increase or decrease the input voltage. The relationship between the input voltage and the output voltage is expressed as follows:

$$\frac{V_{out}}{V_{in}} = \frac{1 - D}{D}. \tag{18}$$

The output voltage  $V_{out}$  of this converter can be higher or lower than the input voltage  $V_{in}$ , depending on the duty cycle  $D$ .

In this paper, a bidirectional DC/DC simulation model is built using MALAB/Simulink. The isolated bidirectional DC/DC voltage converter adopts the phase-shift control method, and the parameters of the simulation model are listed in Table 2.

**Table 2.** Bidirectional DC/DC Simulation Model Parameters.

Parameter	Value
Load Resistor	50 Ω
Voltage input	360 V
Switch Frequency	20 kHz
LVS capacitance C1	20 mF
HVS capacitance C2	10 mF

2.8. Load Model

The load of DC electric propulsion system ships mainly consists of two parts: thrust motor load and daily use load. The thrust motor load has the highest share in the whole ship power system and has the greatest influence on the stability of the ship power grid. The thrust motor of the target ferry adopts permanent magnet synchronous motor, which is a multivariable, strongly coupled nonlinear system [14], and it needs to be simplified to analyze its mathematical model in the  $dq$  coordinate system.

The voltage equation is:

$$\begin{aligned} u_d' &= R_s' i_d + \frac{d\psi_d'}{dt} - \omega_r' \psi_q' \\ u_q' &= R_s' i_q + \frac{d\psi_q'}{dt} - \omega_r' \psi_d' \end{aligned} \tag{19}$$

where  $u_d'$  and  $u_q'$  are voltage's  $dq$  components;  $R_s'$  is motor's stator resistance;  $i_d'$ ,  $i_q'$  are the current's  $dq$  components;  $\psi_d'$  and  $\psi_q'$  are flux chain's  $dq$  components;  $\omega_r'$  is rotor's angular velocity.

The flux chain can be expressed in terms of inductance, which is

$$\begin{aligned} u_d' &= R_s' i_d + L_d' \frac{di_d}{dt} - \omega_r' L_d' i_q \\ u_q' &= R_s' i_q + L_q' \frac{di_q}{dt} - \omega_r' (L_d' i_q + \psi_m') \end{aligned} \tag{20}$$

where  $L_d'$  and  $\psi_q'$  are  $dq$  axis inductance;  $\psi_m'$  is rotor's flux chain.

The motor's equation of motion is shown as

$$\frac{J''}{P_m} \frac{d\omega_r'}{dt} = T_g - F' \frac{\omega_r'}{P_m} - T_L' \tag{21}$$

where  $J''$  is the motor's rotational inertia,  $P_m$  is the motor's pole pairs,  $T_g'$  is the motor's electromagnetic torque,  $F'$  is the damping coefficient, and  $T_L'$  is the motor load torque. The daily load of the ship accounts for a small proportion of the total load, and the modeling is built by using the resistive load module.

### 3. Power Control Strategy for Ship DC Power System

#### 3.1. Diesel Engine's Optimal Speed Seeking Method

In a power supply system that utilizes a variable-speed diesel engine as its power source, the diesel engine's speed control strategy seeks to maintain the engine at its most fuel-efficient operating point for various load conditions. By analyzing the relationship between the specific fuel consumption rate and the speed of the diesel engine under different load conditions, the optimal speed for the engine is determined, and a curve linking the optimal speed points is formed.

This paper used experimental data from the target vessel and a universal performance map to identify optimal speed. Figure 3 presents the universal characteristics curve of the diesel engine of the target vessel, providing a comprehensive understanding of its combustion efficiency characteristics.

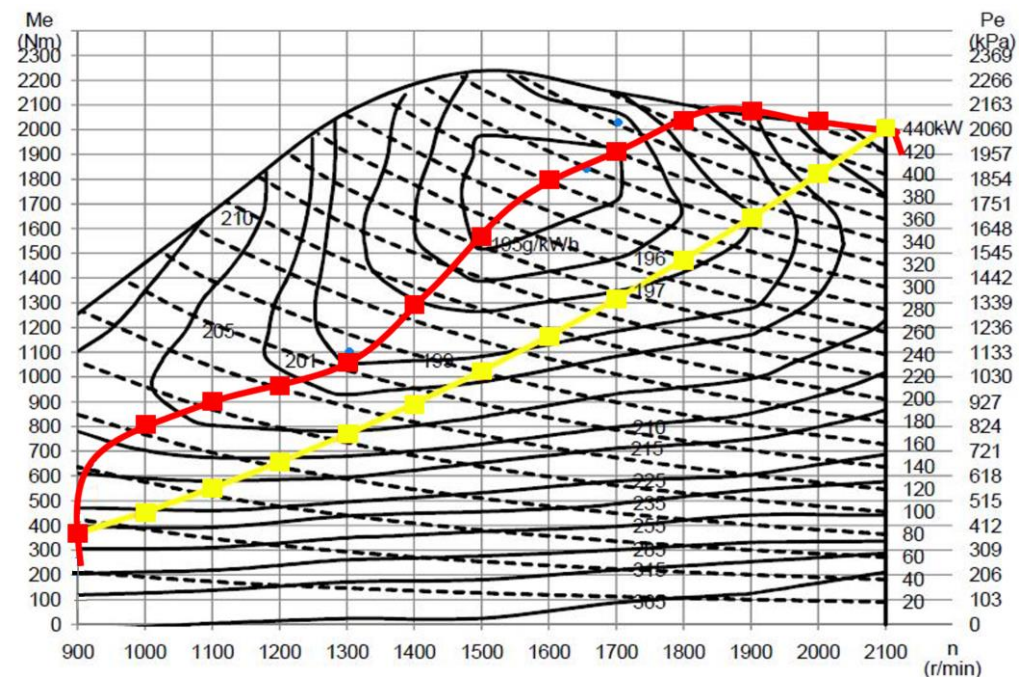


Figure 3. Universal performance map of diesel engine.

The universal performance map synthesizes the load characteristics and speed characteristics curves, providing a comprehensive representation of the engine's main parameters throughout its operating range. It is useful in identifying the most economical operating point of the engine under varying loads. In the case of diesel engines, the uppermost solid curve is the maximum torque curve, also known as the external characteristic curve, which illustrates the maximum torque available at each speed. The effective working area falls below this curve. The solid lines represent equal fuel consumption; each line has a fixed power range expressing the relationship between torque, speed, and specific fuel consumption rate. The dashed line depicts equal power, reflecting the relationship between torque, speed, and power. The yellow line, illustrating the speed curve under normal working conditions before optimization, is optimized to derive the best speed point under different load working conditions. The points connected by the red line show the best acceleration or deceleration curve. The optimized speed curve has a strong fuel-saving potential, albeit with increased response time as compared to the original speed control curve.

In the context of sudden changes in load power, the large inertia, and optimal speed seeking method make it challenging to adjust the speed and output power promptly in response to the load power demand, thereby compromising the quality of power supply to the grid.

This paper proposes the use of supercapacitors to absorb or compensate for the fluctuating power of the DC bus resulting from abrupt load changes. This approach improves bus voltage stability and system safety, allowing the diesel generator set to follow the optimal speed setting curve dynamically and achieve a more economical system.

Effective control of supercapacitor charging and discharging is critical to optimize the operation of the diesel generator set. This paper proposes a control scheme for supercapacitor charging and discharging, depicted in Figure 4. The scheme involves computing the difference between the bus reference voltage  $V_{dc\_ref}$  and the actual voltage value  $V_{dc}$ , which is subsequently fed to the first PI controller to obtain the desired supercapacitor current command. The difference between the output current value and the actual supercapacitor current feeds into the second PI controller, and the resulting output value is compared with a carrying wave to generate the charging and discharging commands for the supercapacitor. The equations are shown as:

$$i_{sc\_ref} = \left( k_{p0} + \frac{k_{i0}}{s} \right) (v_{dcbusref} - v_{dcbus}), \quad (22)$$

$$\mu_{sc\_dcdc\_ref} = \left( k_{p1} + \frac{k_{i1}}{s} \right) (i_{sc\_ref} - i_{sc}), \quad (23)$$

where  $v_{dcbusref}$  is the DC bus reference voltage;  $v_{dcbus}$  is the DC bus's measured voltage;  $i_{sc\_ref}$  is the reference charging or discharging current of supercapacitor;  $i_{sc}$  is the measured current of supercapacitor;  $\mu_{sc\_dcdc\_ref}$  is the reference input of PWM control signal;  $k_{p0}$  and  $k_{p1}$  are the proportionality factors;  $k_{i0}$  and  $k_{i1}$  are the integration factors.

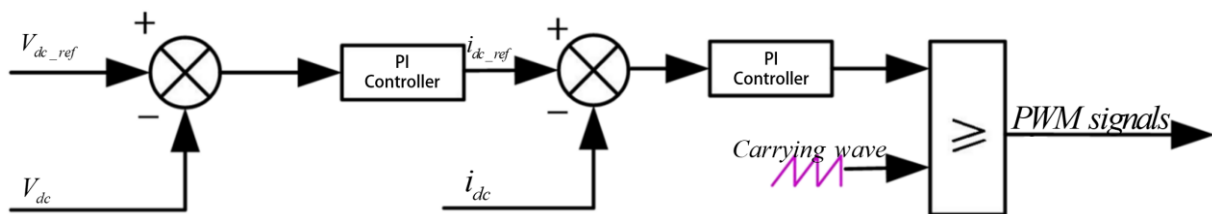


**Figure 4.** Supercapacitor charging and discharging control diagram.

A sudden increase in power load can cause a drop in grid voltage and frequency. To address this, the supercapacitor compensates for the increased power demand, and the diesel engine increases the rack level gradually to speed up output in accord with the optimal fuel consumption curve, thereby achieving dynamic energy saving. Conversely, when the load decreases abruptly, the excess or feedback energy is first absorbed by the supercapacitor. Subsequently, the diesel engine gradually reduces the rack level, slowing down to the target speed in line with the optimal fuel consumption curve.

### 3.2. Droop Control Strategy

The ferry's DC power system has multiple power sources, the diesel generator set is connected in parallel to the DC bus through an AC/DC converter and the supercapacitor through a DC/DC converter. Maintaining a balance between power sources and output power is crucial for the ship's safe operation. In this system, bus voltage and active power have a unique correspondence and bus voltage variation directly reflects the system power balance problem. Droop control, which offers better overall resilience and is suitable for regionally distributed power sources, is the primary control strategy for marine power sources. The traditional droop control method faces an inherent trade-off between achieving higher current distribution accuracy and pursuing smaller voltage deviations. To overcome this limitation, this paper proposes an improved method based on variable droop curve slope and intercept, Voltage offset compensation control and current distribution compensation control are added to the conventional droop control method. The input of voltage offset compensation control is the difference between the monitored voltage of

the DC bus and the set voltage output of the energy management strategy, and the input of current distribution control is the output current of each voltage converter and the set current output of the energy management strategy. as depicted in Figure 5. The variable droop intercept method is effective in suppressing bus voltage drops, while the variable droop slope offers precise power distribution. Secondary control is introduced to adjust the droop curve through compensation methods. This control approach involves adding voltage offset compensation control, using the difference between the measured voltage of the DC bus and the set voltage output of the energy management strategy as input, and current distribution compensation control, which uses the output current of each converter and the set current output of the energy management strategy as input.

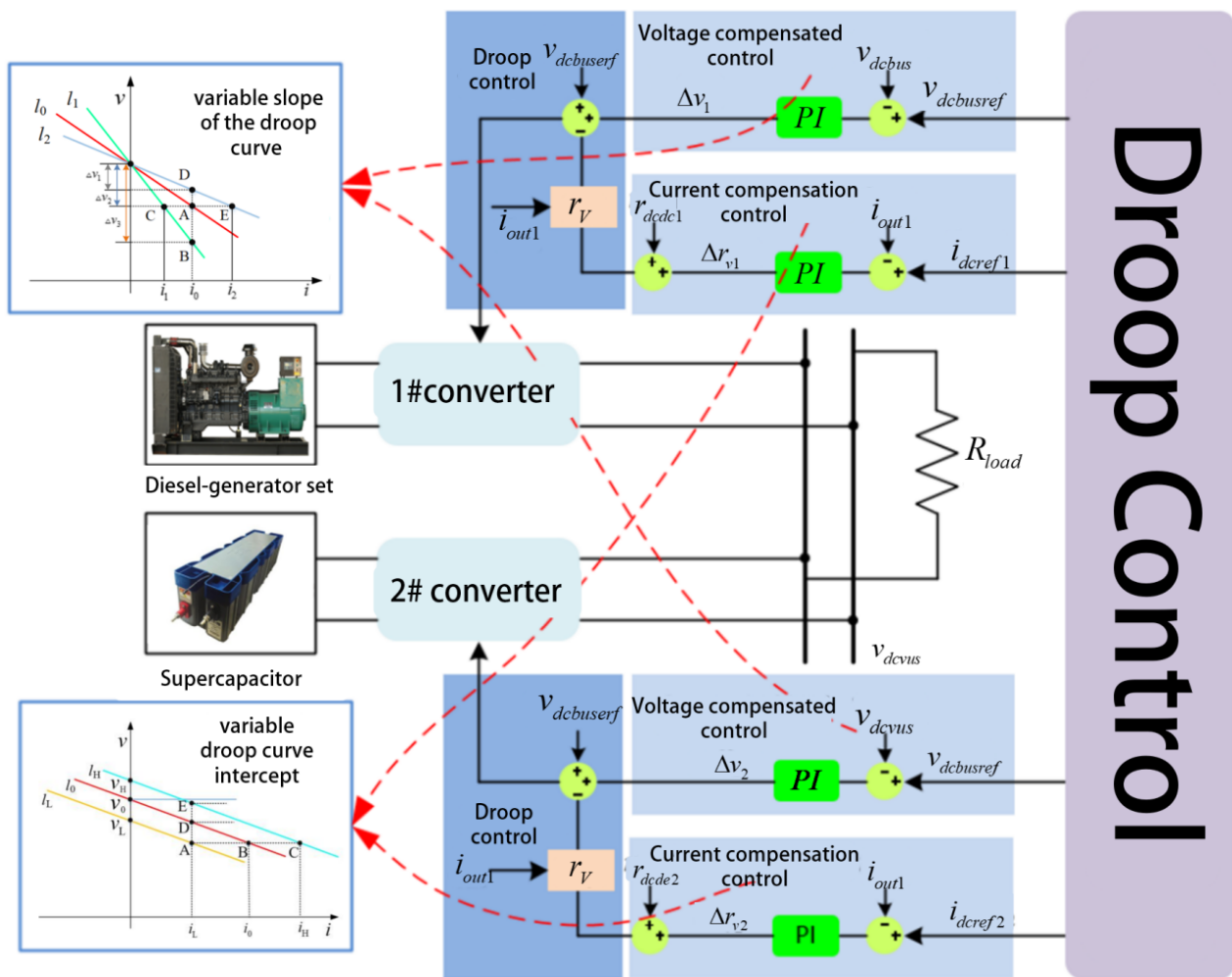


**Figure 5.** Improved droop control strategy based on variable droop curve intercept and variable slope of the droop curve.

The voltage compensation control uses the energy management strategy’s output bus voltage set value as the reference voltage of each converter, and the difference signal between the output voltage of converter No.  $i$  and the set voltage is fed to the PI controller to obtain the compensation voltage  $\Delta v_i$ ,  $\Delta v_i$  can be shown as:

$$\Delta v_i = \left( k_{vp} + \frac{k_{vi}}{s} \right) (v_{dcbusref} - v_{dcbus}), \quad (24)$$

where  $v_{dcbusref}$  is the DC bus set voltage;  $v_{dcbus}$  is the DC bus’s measured voltage;  $k_{vp}$  is the proportionality factor;  $k_{vi}$  is the integration factor.

The current distribution compensation uses a variable droop slope method, which keeps the bus voltage constant and changes the set current of converter No.  $i$  from the energy management strategy, thus enabling the control of different converters' output powers. The signal from the output current of converter No.  $i$  and the set current in the energy management strategy is fed to the PI controller to calculate the compensating droop resistance  $\Delta r_{di}$  of converter No.  $i$ . The variable droop resistance  $r_{vi}$  is obtained by summing the compensating offset resistance and the fixed virtual impedance, which is expressed as:

$$r_{vi} = r_{dc_{dci}} + \left(k_{cp} + \frac{k_{ci}}{s}\right)(r_{dcrefi} - r_{outi}), \quad (25)$$

where  $r_{vi}$  is the variable virtual impedance of converter No.  $i$  and  $r_{dc_{dci}}$  is the fixed virtual impedance of converter No.  $i$ ;  $k_{cp}$  and  $k_{ci}$  are the proportional and integral coefficients in PI control, respectively;  $i_{dcrefi}$  is the reference output current of converter No.  $i$ ; while  $i_{outi}$  is the output current of converter No.  $i$ .

The current distribution compensation and voltage offset compensation can simultaneously achieve effective improvement of power distribution accuracy and effective suppression of bus voltage drops. The improved droop control equation can be expressed as

$$V_{dc} = v_{dc_{busref}} + \Delta v_i - i r_{vi}, \quad (26)$$

where  $V_{dc}$  is the actual voltage of the DC bus.

## 4. Results and Discussions

### 4.1. Simulation Experiments

In order to evaluate the effectiveness of the method presented in this paper, a series of simulation experiments were initially designed, followed by verification on the ferry. The simulation model employed in this study was executed using MATLAB 2019, and the computer processor was the AMD R7 featuring a 3200 MHz CPU. Firstly, the simulation experiments examined the effect of the improved droop control strategy. Subsequently, the study evaluated the ability of the supercapacitor to enhance the grid voltage fluctuation.

#### 4.1.1. Simulation Experiment of Improved Droop Control Strategy

When using droop control to regulate the DC bus voltage, the droop factor  $K_i$  can be determined by the maximum allowable voltage fluctuation value  $\Delta V_{\max}$  of the bus voltage and the maximum current  $I_{\max}$  of the single machine, which is set to  $\pm 3\%$  of the rated DC bus voltage 750 V as the maximum allowable voltage fluctuation value  $\Delta V_{\max}$ , which means  $\Delta V_{\max}$  is 22 V. The maximum and minimum values of DC bus voltage  $V_{dc_{\max}}$  and  $V_{dc_{\min}}$  are 772 V and 728 V, respectively.  $I_{\max}$  can be calculated from the rated power  $P_n$  and  $V_{dc_{\min}}$  of the diesel generator:

$$I_{\max} = \frac{P_n}{V_{dc_{\min}}} = \frac{380000 \text{ W}}{728 \text{ V}} = 522 \text{ A}. \quad (27)$$

The droop factor  $K_i$  is calculated as:

$$K_i = \frac{\Delta V_{\max}}{I_{\max}} = \frac{22 \text{ V}}{522 \text{ A}} = 0.042 \quad (28)$$

The model of the diesel generator set was tested by operating it without the load first, and with 100 kW loaded at 1 s and 2 s, respectively. The aim was to examine the fluctuations of the bus voltage resulting from a load surge while using conventional droop control and the improved droop control method with voltage compensation. The simulation results are shown in Figures 6 and 7, respectively.

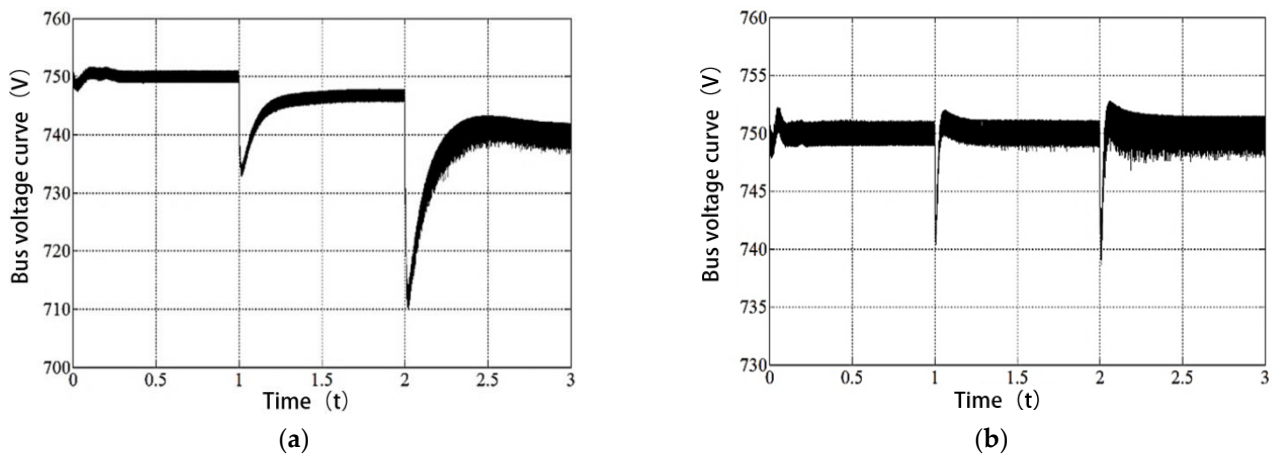


**Figure 6.** (a) DC bus voltage with conventional droop method. (b) DC bus voltage with improved droop control.

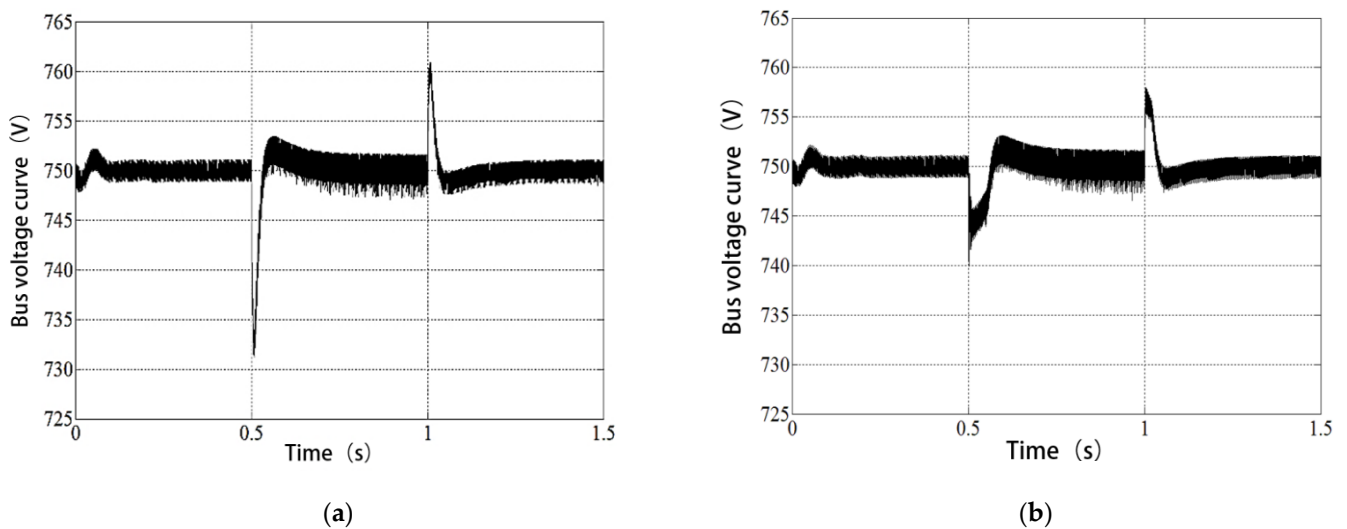


**Figure 7.** (a) DC bus voltage without supercapacitor. (b) DC bus voltage with supercapacitor.

The results from Figure 6a indicate that under conventional droop control, the bus voltage remains around 750 V in the absence of a load. However, when a load of 100 kW is added at 1 s, the bus voltage instantaneously drops and gradually stabilizes after approximately 0.5 s, settling at around 747 V. Moreover, when the total load is increased to 200 kW at 2 s, the voltage drops again and stabilizes at around 740 V. In contrast, as shown in Figure 6b, adopting the improved droop control method with voltage compensation enables the system to stabilize the bus voltage at 750 V for all conditions, regardless of the load size. These simulation experiment results demonstrate that under traditional droop control, an increase in load leads to a decline in bus voltage, whereas the improved droop control method that incorporates voltage compensation can effectively reduce the voltage fluctuation and maintain the bus voltage at the specified value.

#### 4.1.2. Effect of Supercapacitor's Simulation Experiment

To evaluate the supercapacitor's capability to instantaneously compensate for bus voltage deviation during an abrupt load change, a simulation experiment was conducted whereby the diesel generator set was initiated with a 100 kW load, and at 0.5 s, this was increased to 200 kW load, followed by a deload of 100 kW at 1 s. The bus voltage waveform without the use of a supercapacitor is displayed in Figure 7a, whereas that with the incorporation of a supercapacitor is shown in Figure 7b.

The simulation results from Figure 7a indicate that the bus voltage drops to 731 V at the instant that the 200 kW load is introduced to the diesel generator set at 0.5 s, resulting in a 2.5% decrease. Similarly, at 1 s when the 100 kW load is shed, the bus voltage instantly rises by 4.1% to 761 V. On the other hand, in Figure 7b, where the diesel generator set is connected to a supercapacitor, the bus voltage drops by only 1.1% to 742 V at 0.5 s when the 200 kW load is introduced. Moreover, when reducing the system load by 100 kW at 1 s, the voltage instantly rises by 1.1% to 758 V. The simulation results indicate that by incorporating a supercapacitor, the diesel generator set can respond more effectively to sudden load changes, resulting in reduced fluctuations in bus voltage amplitudes, leading to a more stable DC network.

#### 4.2. Performance of Real Ship

An experiment was conducted on the Zhen Yang ferry 3011 to verify the effect of this strategy. The experiment aimed to evaluate the performance of the generator speed when thrust motors changed speeds.

Figure 8a shows the curve of generator speed in the face of load change without the supercapacitor. Under sudden thrust motor's speed acceleration at 14:50:15, the diesel generator's speed was observed to decline from 1088 r/min to 980 r/min, exhibiting a speed fluctuation of around 9.9%. Similarly, under sudden propulsion motor speed deceleration at 14:51:18, the generator speed increased from 1712 r/min to 1791 r/min, with a speed fluctuation of about 4.4%. Figure 8b shows the variation of generator speed under the same operating conditions with supercapacitor and improved droop control. Under similar sudden load increase at 15:04:15, the diesel generator's speed dropped by only 4.5% from 1099 r/min to 1094 r/min, and further reduced the fluctuation range. Likewise, when faced with sudden load decrease at 15:05:15, the generator speed increased by merely 0.9% from 1726 r/min to 1742 r/min. Experiment results suggest that the diesel generators matching with the supercapacitor under the proposed strategy can significantly reduce speed variation, which will be beneficial to power supply.

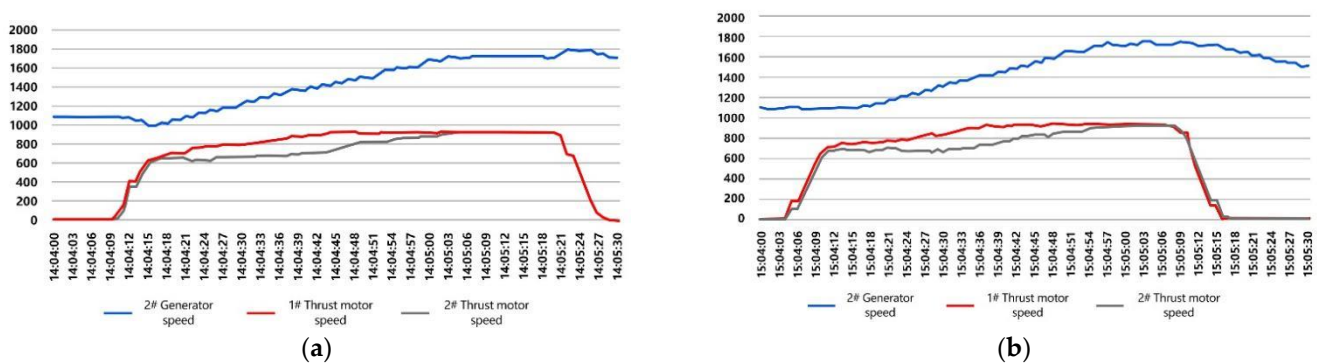


**Figure 8.** (a) speed of generator without supercapacitor. (b) speed of generator with supercapacitor and improved droop control.

## 5. Conclusions

The research in this study focuses on a ferry's DC electric power system, for which a model was constructed to investigate the system's control strategy. To improve grid voltage quality while achieving fuel efficiency, a supercapacitor is implemented to compensate for DC bus energy fluctuations, which operates in conjunction with an improved droop control method with voltage compensation. Both simulation and field tests support the effectiveness of the proposed strategy in addressing large DC bus voltage fluctuation that occurs due to sudden load changes and in ensuring the stability of the power supply.

**Author Contributions:** Conceptualization, L.F.; Methodology, Q.Y. and X.W.; Software, L.C.; Validation, L.F.; Formal analysis, L.C.; Data curation, Q.Y.; Writing—original draft, L.C.; Writing—review & editing, L.F.; Visualization, L.C.; Supervision, Q.Y.; Funding acquisition, Q.Y. All authors have read and agreed to the published version of the manuscript.

**Funding:** This research received no external funding.

**Data Availability Statement:** Not applicable.

**Conflicts of Interest:** The authors declare no conflict of interest.

## Nomenclature

$T_d$	mechanical torque	$C_{sc}$	capacitance capacity of the supercapacitor
$T_f$	friction torque	$U_{scmax}$	supercapacitor's charging cut-off voltage
$T_g$	generator electromagnetic torque	$U_{scmin}$	supercapacitor's discharging cut-off voltage
$J$	rotational inertia	$E_{sc}'$	total available energy
$\omega$	crankshaft angular velocity	$u_a, u_b, u_c$	electromotance of the three-phase AC power
$n$	engine's speed	$L'$	AC input inductance
$L$	output shaft's offset of governor	$Z$	AC line impedance
$P_L$	generator's load power	$i_a, i_b, i_c$	load equivalent resistance electromotive force
$k_i, b_i$	Mechanical torque coefficient of diesel engine	$i_{DC}, u_{DC}$	current and voltage of the DC bus
$M_1^e$	maximum torque of diesel engine	$D$	duty cycle
$L_e$	Maximum travel of governor's output shaft	$V_{out}$	output voltage
$\Delta$	variation of each parameter	$V_{in}$	input voltage
$u(t)$	control injection signal	$u_d', u_q'$	voltage $dq$ components
$e(t)$	speed deviation;	$R_s'$	resistance of motor stator
$K_P, T_I, T_D$	PID control parameters.	$i_d', i_q'$	current's $dq$ components
$F(s)$	fuel rack's position	$\psi_d', \psi_q'$	flux chain's $dq$ components
$K$	proportionality coefficient	$\omega_r'$	motor's rotor angular velocity.
$T(s)$	actuator inertia time constant	$L_d', L_q'$	$dq$ inductance
$\psi_{sd}, \psi_{sq}$	stator flux's $dq$ components	$\psi_m'$	rotor's flux chain.
$\psi_{rd}, \psi_{rq}$	rotor flux's $dq$ components	$J''$	motor's rotational inertia
$L_s$	stator self-inductance coefficient	$P_m$	pole pairs of thrust motor
$L_r$	rotor self-inductance coefficient	$F'$	damping coefficient
$L_m$	stator-rotor mutual inductance coefficient	$T_L'$	motor's load torque
$i_{sd}, i_{sq}$	stator current's $dq$ components	$U_{dc\_ref}$	DC bus reference voltage
$i_{rd}, i_{rq}$	rotor current's $dq$ components	$V_{dc}$	actual voltage value
$U_s, U_r$	instantaneous phase voltage of the stator and rotor	$v_{dcbusref}$	DC bus reference voltage
$R_s, R_r$	resistance of the stator and rotor	$v_{dcbus}$	DC bus's measured voltage;
$L_s, L_r$	stator and rotor self-inductance	$i_{sc\_ref}$	reference charging or discharging current of supercapacitor
$i_s, i_r$	stator and rotor current	$i_{sc}$	current of supercapacitor
$\omega_r$	rotor angular velocity	$\mu_{sc\_dcdc\_ref}$	reference input of PWM control signal
$\theta$	angle between the stator and rotor	$k_{p0}, k_{p1}$	proportionality factors
$\omega_1$	synchronous angular velocity of stator frequency	$k_{i0}, k_{i1}$	integration factors
$\omega_s$	slip of the asynchronous motor	$k_{vp}$	proportionality factor
$\omega_z$	stator's angular speed	$k_{vi}$	integration factor
$p$	coefficient of differentiation	$r_{vi}$	variable virtual impedance of converter No. $i$
$P_g$	polar pairs of generator	$r_{dcdci}$	fixed virtual impedance of converter No. $i$ .
$T_L$	load torque	$k_{cp}, k_{ci}$	proportional and integral coefficients in PI control
$J'$	generator's rotational inertia	$i_{dcrefi}$	reference output current of converter No. $i$
$u_d, u_q$	stator voltage $dq$ components	$i_{outi}$	output current of converter No. $i$
$\omega_e$	electric angular velocity	$V_{dc\_max}, V_{dc\_min}$	maximum and minimum values of DC bus voltage
$\sigma$	leakage coefficient	$I_{max}$	maximum current of the single machine,
$U_c$	terminal voltage of the supercapacitor bank	$P_n$	rated power of thrust motor
$E_{sc}$	stored energy		

## References

1. Ma, W.M. Typical applications of power electronics in naval ship power systems. *Trans. China Electrotech. Soc.* **2011**, *26*, 1–7. (In Chinese)
2. Chen, J.; Cao, X.; Chen, X.; Guo, A. Comparative Study on AC and DC Electric Propulsion Systems of Ship. *Mar. Electr. Electron. Eng.* **2019**, *39*, 11–13. [[CrossRef](#)]
3. Xiao, Z.; Zhu, H.; Cao, J.; Xu, R.; Zhang, S. High-Efficiency Operation Control of DC Shipboard Grid Supplied by Diesel Gensets with Active Front End. *Proc. CSU-EPSSA* **2023**, 1–9. [[CrossRef](#)]
4. Huang, K.; Li, Y.; Zhang, X.; Liu, L.; Zhu, Y.; Meng, X. Research on power control strategy of household-level electric power router based on hybrid energy storage droop control. *Prot. Control Mod. Power Syst.* **2021**, *6*, 13. [[CrossRef](#)]
5. Geertsma, R.D.; Negenborn, R.R.; Visser, K.; Hopman, J.J. Design and control of hybrid power and propulsion systems for smart ships: A review of developments. *Appl. Energy* **2017**, *194*, 30–54. [[CrossRef](#)]
6. Tang, D.; Yan, X.; Yuan, Y.P. Power Management Technology in Ship's Integrated Power System. *Navig. China* **2017**, *40*, 56–60.
7. Wilhelm, J.; Janssen, H.; Mergel, J.; Stolten, D. Energy management for a fuel cell/battery hybrid system. In Proceedings of the 2010 Emobility—Electrical Power Train, Leipzig, Germany, 8–9 November 2010; pp. 1–6.
8. Caparrós Mancera, J.J.; Saenz, J.L.; López, E.; Andújar, J.M.; Manzano, F.S.; Vivas, F.J.; Isorna, F. Experimental analysis of the effects of supercapacitor banks in a renewable DC microgrid. *Appl. Energy* **2022**, *308*, 118355. [[CrossRef](#)]
9. Salih, H.W.; Wang, S.; Farhan, B.S. Optimum Control Strategy of MTG—Grid Tie with Isolated Dc Grid Using GA-PI and Bidirectional Svpwm Converter. In Proceedings of the 2017 2nd Joint International Information Technology, Mechanical and Electronic Engineering Conference (JIMEC 2017), Chongqing, China, 4–5 October 2017.
10. Liu, X.; Gao, Z. Large signal stability analysis of DC microgrid system considering dynamic characteristics of constant power load and energy storage system. *Trans. China Electrotech. Soc.* **2019**, *34* (Suppl. S1), 292–299.
11. Wang, H.; Chen, J.; Li, B. Large disturbance stability analysis of DC microgrid based on improved droop control. In Proceedings of the 2018 China International Conference on Electricity Distribution (CICED), Tianjin, China, 17–19 September 2018.
12. Yu, S.; Mi, Y.; Ma, Y. Power distribution control of an island DC microgrid based on adaptive high-pass filter droop control. *Power Syst. Prot. Control* **2020**, *48*, 19–26.
13. Wang, Y.; Xu, K.; Chen, J. Dual-phase-shifting optimization control of isolated DC-DC converter. *Electr. Mach. Control* **2017**, *21*, 53–61, 71.
14. Zhou, Z.; Camara, M.B.; Dakyo, B. Coordinated Power Control of Variable-Speed Diesel Generators and Lithium-Battery on a Hybrid Electric Boat. *IEEE Trans. Veh. Technol.* **2017**, *66*, 5775–5784. [[CrossRef](#)]

**Disclaimer/Publisher's Note:** The statements, opinions and data contained in all publications are solely those of the individual author(s) and contributor(s) and not of MDPI and/or the editor(s). MDPI and/or the editor(s) disclaim responsibility for any injury to people or property resulting from any ideas, methods, instructions or products referred to in the content.